



Research Article

Volume 3 - Issue 2: 50-56 / April 2020

# INVESTIGATION OF THE FLOW OVER NACA 63-415 AIRFOIL

Onur ERKAN<sup>1\*</sup>, Musa ÖZKAN<sup>1</sup>

<sup>1</sup>Department of Mechanical Engineering, Bilecik Seyh Edebali University, 11230, Bilecik, Turkey

**Received:** November 07, 2019; **Accepted:** December 28, 2019; **Published:** April 01, 2020


## Abstract


In this article, a two-dimensional, incompressible flow around a NACA 63-415 airfoil, which is widely used as one of the commercial wind turbine blade profiles, is investigated. The goal of this research is to obtain the optimum angle of attack for this particular type of airfoil within a precise range. The Reynolds-Averaged Navier-Stokes (RANS) technique of Computational Fluid Dynamics (CFD) has been employed to examine the flow where the Reynolds number is in the range of  $10^5$  to  $3 \times 10^6$  and also for the angles of attack from  $0^\circ$  to  $20^\circ$ . These are the typical flow conditions mostly encountered in the real applications of wind turbine blades. The turbulent flow is modelled by means of the Spalart-Allmaras turbulence model since its capability of simulating aerodynamic flows. The ratio of the lift force to the drag force acting on the airfoil has been chosen as a control parameter since the lift force increases the power generated by the turbine, whereas the drag force negatively affects the performance. The present numerical result shows that the maximum lift to drag ratio is observed between  $2.5^\circ$  and  $3.5^\circ$ , depending on the Reynolds number.

**Keywords:** Angle of attack, CFD, NACA airfoil, Renewable energy, Spalart-Allmaras model, Wind turbines

\*Corresponding author: Department of Mechanical Engineering, Bilecik Seyh Edebali University, Bilecik, 11230, Turkey

E mail: onur.erk@bilecik.edu.tr (O. ERKAN)

Onur ERKAN  <https://orcid.org/0000-0001-7488-8039>

Musa ÖZKAN  <https://orcid.org/0000-0002-1322-3276>

Cite as: Erkan O, Özkan M. 2020. Investigation of the flow over NACA 63-415 airfoil. BSEng Sci, 3(2): 50-56.

## 1. Introduction

The global demand for energy has been increasing since the Industrial Revolution. Recently, this demand has significantly raised as a result of the increase in the world's population and the substantial need for energy in heavy industry and transportation. The fossil fuels have been the main source to produce energy until quite recently. The use of fossil fuels results in several disasters such as global warming, climate change and wars resulted from energy crises. As a result, the use of alternative resources of energy has become an extremely important topic in the sense of the global policy on protecting the future of the world. By means of this motivation the proportion of the power generated by renewable

resources has reached up to approximately 10.4% in the worldwide total energy production (REN21, 2018).

The renewable resources can be classified as solar, wind, biomass, hydraulic, geothermal and marine energy. The wind energy, particularly, is one of the most important renewable resources because of its unlimited and approximately continuous nature. Hence, the generation of electricity by means of the wind has reached up to 5.6% in the total electricity production from the renewable resources (REN21, 2018).

Although the potential of wind energy has been recognized, several restraints may be encountered during the generation of electricity. The first restriction is the Betz limit which is the theoretical maximum efficiency of the wind turbine (Betz, 1966). This limitation defines that

the only 59.3% of the kinetic energy from wind can be used to generate electricity since simply in terms of the conservation of momentum, some air should pass through the turbine to spin the blades. In addition to this theoretical limitation, there are other inevitable restrictions such as the design parameters of the wind turbine and surface roughness which may be caused by dust, insects, icing, erosion or surface finishing (Sagol et al., 2013).

In terms of the design parameters, the angle of attack is one of the very most important and thus has been widely studied in previous research. Its importance comes from its direct relation with the aerodynamic forces shown in Figure 1.

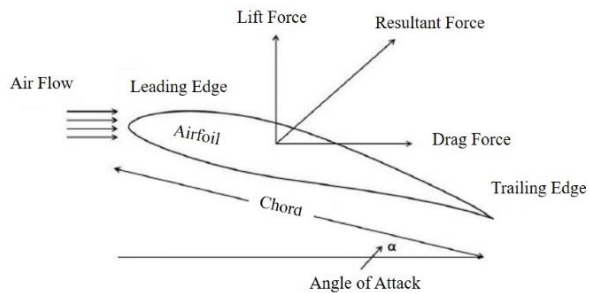


**Figure 1.** Forces acting on an airfoil (Panigrahi and Mishra, 2014).

These aerodynamic forces are crucial since the lift force rotates the blades of the turbine and thus generates electricity, whereas the drag force slows down this rotation which is a negative effect on the generation of electricity. The non-dimensional form of the lift and drag forces are represented by the lift ( $C_L$ ) and the drag coefficients ( $C_D$ ) which are given by Equation 1 and 2, respectively (Burton et al., 2011). Here,  $\rho$  is the density of air,  $A_L$  is the projected wing area,  $A_D$  is the cross-sectional area and  $V$  is the velocity of air. Due to the fact that the angle of attack,  $\alpha$ , directly and crucially affects the lift and drag coefficients, researchers have often investigated the relation between them. The ratio of the lift force to the drag force is called the lift to drag ratio and it is used as a control parameter in this study. It is beneficial to examine the effect of the angle of attack on the lift to drag ratio rather than investigating the effects on both forces separately. This approach has previously been employed by several different studies in literature (Chakroun et al., 2004; Hafiz et al., 2012; Sayed et al., 2012; Chaudhary and Nayak, 2015; Patil and Thakare, 2015). The generation of electricity, i.e. the performance of the wind turbine, is increased when the lift to drag ratio is increased.

$$C_L = \frac{F_L}{\frac{1}{2} \rho A_L V^2} \quad (1)$$

$$C_D = \frac{F_D}{\frac{1}{2} \rho A_L V^2} \quad (2)$$

Due to the fact that there is an important relation between the lift to drag ratio, and thus the efficiency of the wind turbine, and the angle of attack, this important design parameter needs to be carefully investigated for each type of blades that are used as wind turbine blades. National Advisory Committee for Aeronautics (NACA) 63-415 airfoil, as one of these turbine blades, has been rarely examined in literature. Additionally, studies in literature have reported inconsistent results where the optimum angle of attack is in the range of  $2^\circ$  to  $14^\circ$  (Vendan et al., 2010; Chaudhary and Nayak, 2015; Yilmaz et al. 2016). Therefore, a detailed examination is still necessary for this particular type of the blade to ensure the optimum angle of attack in a precise range.

Consequently, for the determination of the optimum angle of attack for the NACA 63-415 airfoil, various Reynolds numbers range from  $10^5$  to  $3 \times 10^6$  have been investigated and the angle of attack differs between  $0^\circ$  and  $20^\circ$  as these are the most commonly encountered flow conditions in real wind turbine applications (Timmer and Rooji, 2003; Sayed et al., 2012; Salem et al., 2013).

## 2. Material and Method

In this research, the flow over a wind turbine blade has been investigated by means of CFD approach. The flow has been assumed to be two-dimensional, steady state and incompressible. NACA 63-415 airfoil, which is generally used as wind turbine blades, was chosen for the analyses (Hochart et al., 2008). So, firstly, the details of NACA 63-415 airfoil is described in the following section and thereafter the governing equations, the turbulence model and the numerical model are described.

### 2.1. The Airfoil

To design an efficient wind turbine, determining a suitable airfoil is one of the most important issues. The blade sections of almost all wind turbines are either created from NACA airfoils or designed according to them (Abbott and Von Doenhoff, 1959). NACA airfoils are quite common since there is high quality experimental data which was presented by the NACA (Burton et al., 2011). There are various series of NACA airfoils. In this paper, NACA 63-415 type of airfoil from the NACA 6 series has been used since it is proved that NACA 63-415 airfoil has good stall characteristics. Furthermore, it is often used for small planes and stall regulated wind turbines (Hansen, 2008). Each number in the name of the airfoil refers to a characteristic of the airfoil:

- The first number states series of airfoil {6}.
- The second number means the distance of the minimum pressure area in tens of percent of chord {3}.
- The third number means lift coefficient in tenths {4}.
- The last two numbers indicate percent of maximum thickness to chord length ratio {15} (Abbott and Von Doenhoff, 1959; Kuethe and Chow, 1998).

## 2.2. Governing Equations

The governing equations, for the steady-state, incompressible turbulent flow over the airfoil, are the steady-state Reynolds-averaged Navier-Stokes (RANS) equations. The conservation of mass and momentum are given by Equation 3 and Equation 4, respectively (Batchelor, 1967; Mulvany et al., 2004; ANSYS Inc., 2013).

$$\frac{\partial(\rho u_i)}{\partial x_i} = 0 \quad (3)$$

$$\frac{\partial(\rho u_i u_j)}{\partial x_j} = -\frac{\partial p}{\partial x_i} + \frac{\partial}{\partial x_i} \left[ \mu \left( \frac{\partial u_i}{\partial x_j} + \frac{\partial u_j}{\partial x_i} - \frac{2}{3} \delta_{ij} \frac{\partial u_l}{\partial x_l} \right) \right] + \frac{\partial}{\partial x_j} (-\rho \overline{u_i' u_j'}) \quad (4)$$

Here,  $\rho$  is the density,  $p$  is the pressure,  $\mu$  is the dynamic viscosity, and  $(-\rho \overline{u_i' u_j'})$  is the Reynolds stresses. In Reynolds averaged methods, Reynolds stresses need to be properly modelled in order to successfully model turbulent flow. A common technique employs the Boussinesq hypothesis to correlate the Reynolds stresses with the mean velocity gradients as the relation is formulated in Equation 5 (Hinze, 1975).

$$-\rho \overline{u_i' u_j'} = \mu_t \left( \frac{\partial u_i}{\partial x_j} + \frac{\partial u_j}{\partial x_i} \right) - \frac{2}{3} (\rho k + \mu_t \frac{\partial u_l}{\partial x_l}) \delta_{ij} \quad (5)$$

Here, the turbulent (eddy) viscosity  $\mu_t$  and the turbulent kinetic energy  $k$  need to be obtained via additional transport equations. These additional transport equations are obtained by means of the turbulence model selected. This paper employs the Spalart-Allmaras model to simulate the turbulent flow.

## 2.3. Spalart-Allmaras Turbulence Model

There are different methods to investigate turbulent flows such as Direct Numerical Simulation (DNS) and Large Eddy Simulation (LES) but the DNS and LES analyses requires large solution time. Therefore, it is more useful to model the turbulent flows instead of solving the whole characteristics of these flow types. These mathematical models for solving turbulent flows are called turbulence models. In this investigation, the Spalart-Allmaras turbulence model has been used for modelling the flow around the airfoil.

The Spalart-Allmaras model is in the group of turbulence models which has one transport equation. The only transport equation in this model solves the kinematic eddy viscosity ( $\tilde{\nu}$ ). Differently from other one equation turbulence models, the Spalart-Allmaras model is more practical and has more accurate results. Moreover, this turbulence model provides higher accuracy for the analysis of boundary layers which are exposed to reverse pressure gradients. Hence, it is often used for especially aerospace applications and wind turbine aerodynamics (Wilcox, 2006). The transport equation for the kinematic

eddy viscosity ( $\tilde{\nu}$ ) solved by the Spalart-Allmaras turbulence model is given by Equation 6.

$$\frac{\partial \tilde{\nu}}{\partial t} + U_j \frac{\partial \tilde{\nu}}{\partial x_j} = c_{b1} \tilde{\nu} \tilde{S} - c_{\omega 1} f_{\omega} \left( \frac{\tilde{\nu}}{d} \right)^2 + \frac{1}{\sigma} \frac{\partial}{\partial x_k} \left[ (\nu + \tilde{\nu}) \frac{\partial \tilde{\nu}}{\partial x_k} \right] + \frac{c_{b2}}{\sigma} \frac{\partial \tilde{\nu}}{\partial x_k} \frac{\partial \tilde{\nu}}{\partial x_k} \quad (6)$$

## 2.4. CFD Model

Firstly, the geometry of the 2D wind turbine blade profile was generated from the coordinate points of NACA 63-415 airfoil. The chord length ( $c$ ) of the blade is 0.1 m. The computational area was created as shown in Figure 2 where the dimensions are given as a  $12.5c$  radius of the half circle,  $25c$  in height and  $20c$  in length of the rectangle. In the analyses, C-type mesh was used because this type of mesh reduces the solution time by means of decreasing the number of equations to be solved (Ferrer and Munduate, 2009; Gharali and Johnson, 2012). In order to analyse the boundary layer and to determine vortices which appear at the back of the airfoil, the fine mesh was created at around and rear of the airfoil. The mesh structure was modified gradually for the mesh independence test whose details will be given in Section 3.1. After the mesh independence test, the mesh structure which has been decided to use in analyses is shown in Figure 3.

The velocity inlet boundary condition was assigned to Section A and the pressure outlet boundary condition was assigned to Section B shown in Figure 2. Also, the airfoil surface was assigned as a smooth wall with a no-slip condition. The velocity inlet boundary condition was determined according to the 5 different Reynolds numbers which are  $Re=10^5$ ,  $5 \times 10^5$ ,  $7 \times 10^5$ ,  $10^6$  and  $3 \times 10^6$ . The pressure outlet boundary condition was set as gauge pressure of 0 Pa which represents the normal atmospheric pressure. It was considered that thermophysical properties of air are at a sea level condition. In the analyses, Spalart-Allmaras turbulence model was used.

## 3. Results

### 3.1. Mesh Independence Test

The discretization process of the CFD model directly affects the results acquired by means of the related mesh structure. Therefore, a mesh independence test has been performed before starting the main analyses. The size of a mesh element has been gradually reduced and at every iteration of this reduction, a control parameter such as the lift coefficient, pressure and/or temperature has been compared with the result of the former grid size. This procedure has been followed until the control parameter remains constant between the iterations

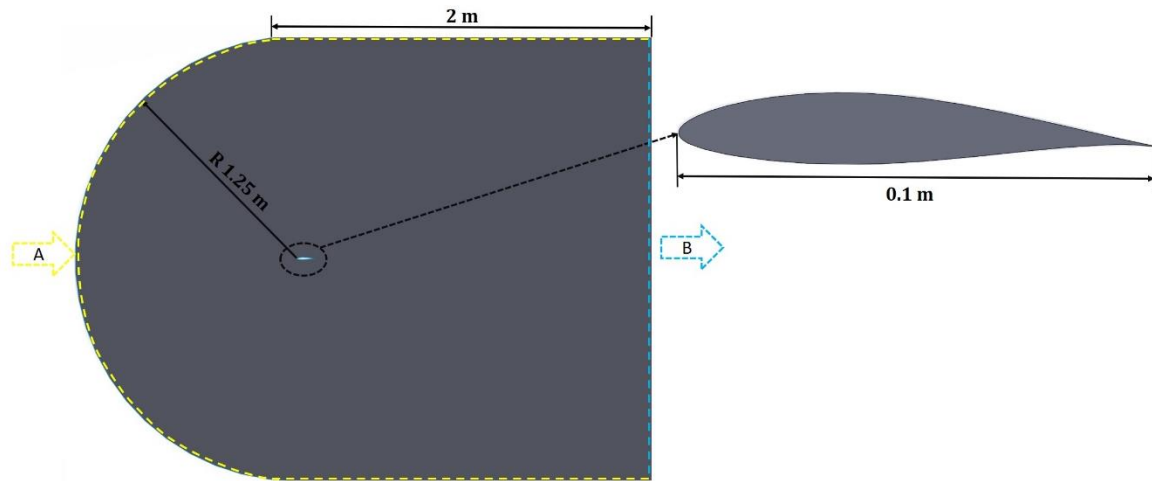


**Figure 2.** The CFD model and boundary conditions.

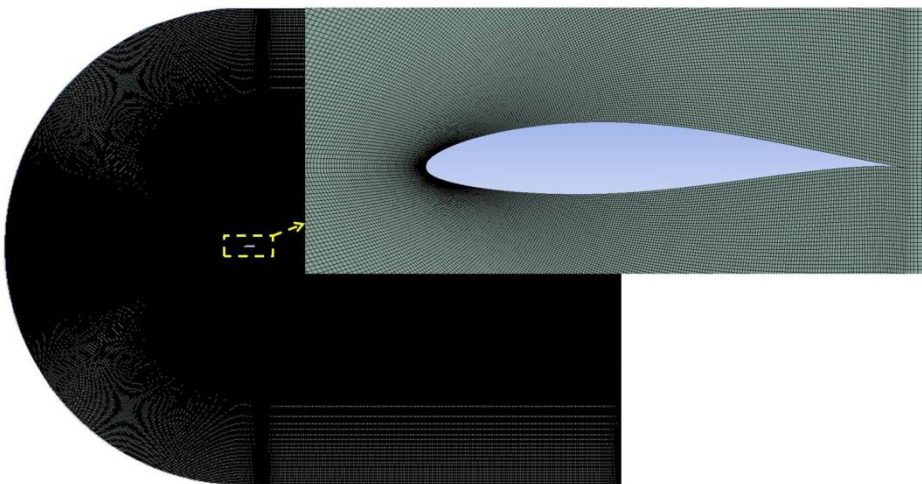


**Figure 3.** C-type structured mesh used for CFD analyses.

In the current study, firstly, a rough structure of mesh which has approximately 16000 number of elements was generated and then the quality of the mesh structure was gradually improved.

The number of mesh elements has been reached approximately 700000 at the end of the mesh independence test. The lift and drag coefficients were chosen as control parameters between the iterations of the mesh improvements. The mesh independence test was carried out at  $Re=10^5$  and  $\alpha=5^\circ$ . The Spalart-Allmaras turbulence model was used for the mesh independence test.

Furthermore, the non-dimensional wall distance ( $y^+$ ) is a significant criterion for the investigation of turbulence flows, particularly the flows affected crucially by the boundary layer. Salem et al. (2013) recommended that, for the particular boundary layer flows mentioned, the wall ( $y^+$ ) value needs to be between 1 and 5. Therefore, in the present study, the quality of the mesh structure in the vicinity of the wall was increased and by this means the wall ( $y^+$ ) value was achieved to be in the reported limitation.

As previously mentioned, the control parameters are the lift coefficient and the drag coefficient. Figure 4 illustrates the variation of the values of the lift coefficient and the drag coefficient with the number of mesh elements. It can be seen from the figure that their value remains approximately constant at 0.8 and 0.013, respectively, after the number of the mesh elements reached 218163. Considering these results, it was decided that the results would be independent from mesh structures for number of the mesh elements 218163 and above. Thus, the mesh structure which has 322806 number of elements has been employed for the current analyses.

### 3.2. Validation of the Numerical Results

In this study, the analyses were performed at 5 different Reynolds numbers and 20 different angles of attack. For the validation of the CFD analyses the present numerical results, which were obtained at  $Re=3 \times 10^6$ , have been compared with the experimental results of Abbott and Von Doenhoff (1959), see Figure 5. Also, the current results, which were obtained at  $Re=5 \times 10^5$ , have been compared with the numerical results of Villalpando et al. (2012) and this comparison is shown in Figure 6. As a

result of these comparisons, it can be concluded that the present numerical results are reasonably consistent with the literature data and thus the analyses are reliable.

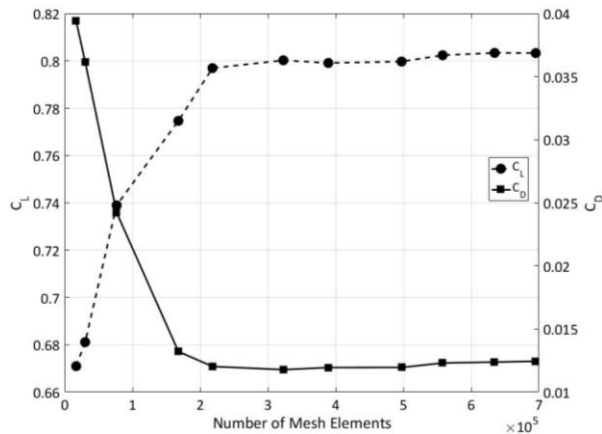


Figure 4. The results of the mesh independence test.

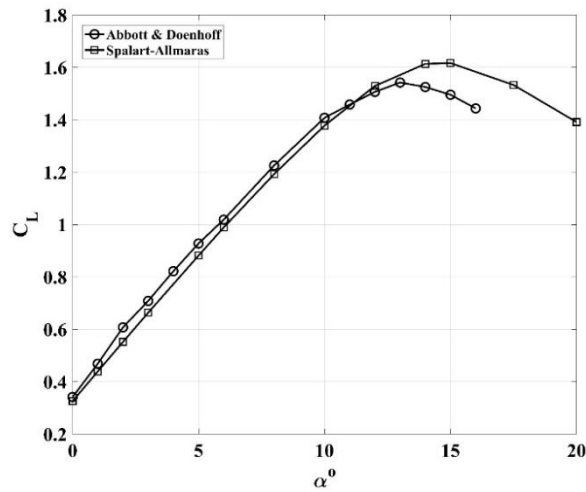


Figure 5. Comparison between computational results of the current study (Spalart-Allmaras) and the experimental data of Abbott and von Doenhoff (1959).

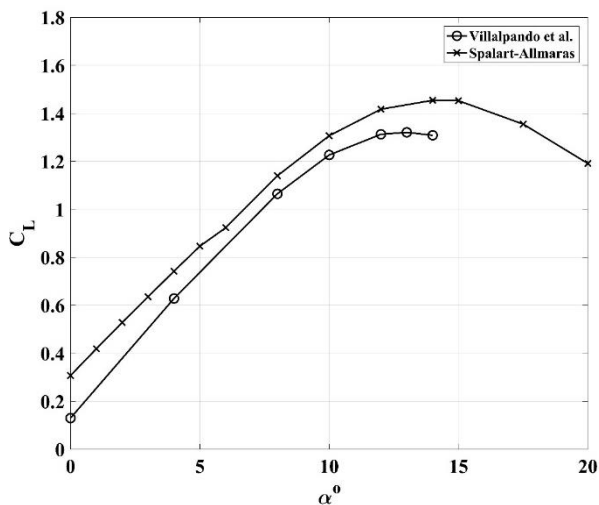


Figure 6. Comparison between the computational data of the current study (Spalart-Allmaras) and the numerical data of Villalpando et al. (2012).

### 3.3. Optimum Angle of Attack

The results of the lift coefficient are shown in Figure 7. It can be seen from this figure that the lift coefficient is increased with an increase in the Reynolds number. This increase continues until the angle of attack reaches 15°. After this value of the angle of attack, the lift coefficient begins to drop because of the boundary layer separation.

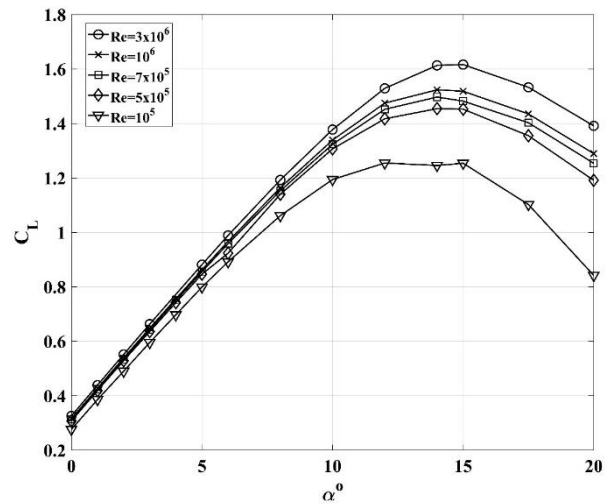


Figure 7. The change in the lift coefficient  $C_L$  by the angle of attack  $\alpha^\circ$ .

On the other hand, the drag coefficient is decreased with an increase in the Reynolds number, as shown in Figure 8. Similar to the lift coefficient, the drag coefficient is increased until the angle of attack reaches 15°. On the contrary to the lift coefficient, the drag coefficient is increased rapidly when the angle of attack reaches above 15° as a result of the boundary layer separation.

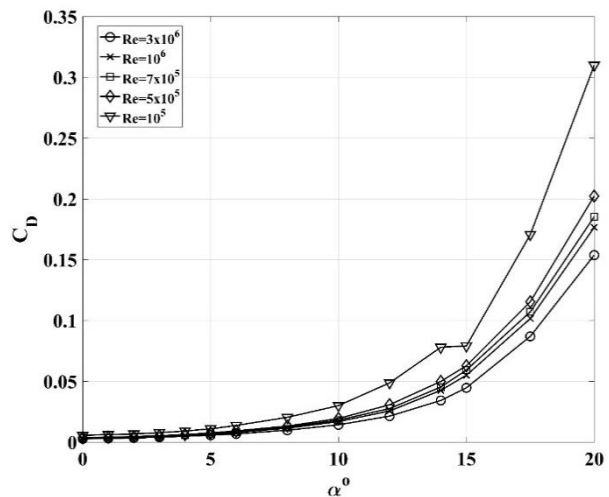


Figure 8. The change in the drag coefficient  $C_D$  by the angle of attack  $\alpha^\circ$ .

Considering the lift and drag coefficients separately may not give enough insights into the performance of the airfoil. Thus, as previously mentioned, the lift to drag ratio has been examined and the change of this parameter with

the angle of attack is shown in Figure 9. One can recognize from this figure that the maximum range for the lift to drag ratio appears to be between 2° and 3.5°. The optimum angle of attack for NACA 63-415 airfoil was previously reported as between 2° and 5.25° (Vendan et al., 2010; Chaudhary and Nayak, 2015). The new result of the present study provides the optimum range for the angle of attack more accurate than the previous literature data. Moreover, it can be observed that the lift to drag ratio is increased with an increase in the Reynolds number.

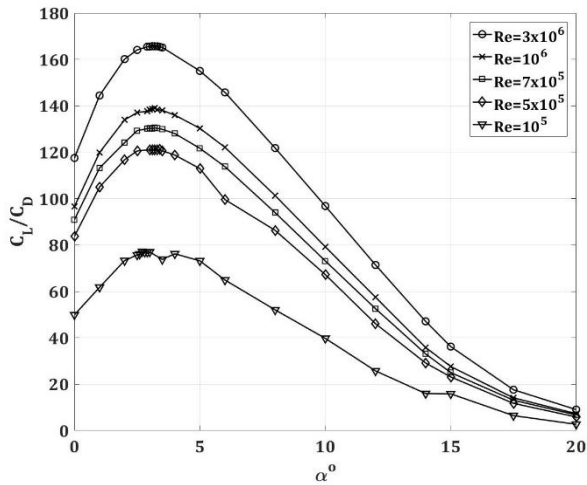


Figure 9. The lift to drag ratio  $C_L/C_D$  as a function of the angle of attack  $\alpha^\circ$ .

#### 4. Discussion

In the current investigation, a 2D, steady-state, incompressible flow over NACA 63-415 was investigated by means of the RANS approach of a CFD application. The analyses were performed between  $Re=10^5$  and  $Re=3 \times 10^6$  and also for the angles of attack range from 0° to 20°. Thus, 100 different numerical analyses were carried out in total. The Spalart-Allmaras turbulence model was used. The comparison between the available numerical and experimental data in literature and the results of the present study revealed that the Spalart-Allmaras turbulence model is suitable for solving this type of flow problems.

Consequently, it was observed that the lift coefficient is increased with an increase in the Reynolds number. On the other hand, the drag coefficient is decreased with an increase in the Reynolds number. Moreover, the increase of the angle of attack until 15° raises the lift coefficient but the lift coefficient is decreased rapidly for the angles of attack greater than 15°. Also, the drag coefficient is increased very fast for the angles of attack above 15°. These rises and declines in the coefficients were caused by the pressure drop and the vortices appear downwards to the airfoil due to the boundary layer separation.

The main result of this current investigation is that the optimum angle of attack ranges from 2.5° to 3.5°

depending on Reynolds number for this airfoil. This optimum range of the angle of attack has been acquired by means of the evaluation of the lift to drag ratio. Due to the fact that this range was previously stated between 2° and 5.25° in literature, the present study can provide more accurate and specific optimum working conditions for the wind turbines using NACA 63-415 airfoil as blades.

#### Conflict of interest

The authors declare that there is no conflict of interest.

#### References

- Abbott IH, Von Doenhoff AE. 1959. Theory of Wing Sections, Including a Summary of Airfoil Data. New York, USA: Courier Corporation.
- ANSYS Inc. 2013. ANSYS fluent 15.0 theory guide Tech. rep. Canonsburg, PA, USA.
- Batchelor GK. 1967. An introduction to fluid dynamics. Cambridge, UK: Cambridge University Press.
- Betz A. 1966. Introduction to the Theory of Flow Machines. Oxford, UK: Pergamon Press.
- Burton T, Jenkins N, Sharpe D, Bossanyi E. 2011. Wind Energy Handbook. 2nd ed. West Sussex, UK: John Wiley & Sons.
- Chakroun W, Al-Mesri I, Al-Fahad S. 2004. Effect of surface roughness on the aerodynamic characteristics of a symmetrical airfoil. Wind Eng, 28(5): 547-564.
- Chaudhary U, Nayak SK. 2015. Micro and small-scale HAWT blades airfoils study through CFD for low wind applications. In 2015 Annual IEEE India Conference; 17-20 December 2015, New Delhi, India.
- Ferrer E, Munduate X. 2009. CFD Predictions of transition and distributed roughness over a wind turbine airfoil. 47th AIAA Aerospace Sciences Meeting Including the New Horizons Forum and Aerospace Exposition; 05 -08 January 2009, Orlando, Florida, USA.
- Gharali K, Johnson DA. 2012. Numerical modeling of an S809 airfoil under dynamic stall, erosion and high reduced frequencies. Ap Energy, 93: 45-52.
- Hafiz M, Noh M, Hussein A, Hamid A, Helmi R, Wirachman W, Mohd SN. 2012. Wind tunnel experiment for low wind speed wind turbine blade. In Ap Mec and Mat, 110: 1589-1593.
- Hansen MOL. 2008. Aerodynamics of Wind Turbines. 2nd ed. London, UK: Earthscan.
- Hinze JO. 1975. Turbulence. New York, USA: McGraw-Hill Publishing Co.
- Hochart C, Fortin G, Perron J, Ilinca A. 2008. Wind turbine performance under icing conditions. Wind Energy: An IJPAWPCT, 11(4): 319-333.
- Kuethe AM, Chow CY. 1998. Foundations of Aerodynamics. 5th ed. New York, USA: John Wiley & Sons.
- Mulvany NJ, Chen L, Tu JY, Anderson B. 2004. Steady-state evaluation of two-equation RANS (reynolds-averaged navier-stokes) turbulence models for high-Reynolds number hydrodynamic flow simulations Tech. rep. Victoria, Australia.
- Panigrahi DC, Mishra DP. 2014. CFD simulations for the selection of an appropriate blade profile for improving energy efficiency in axial flow mine ventilation fans. J Sust Mining, 13(1): 15-21.
- Patil BS, Thakare HR. 2015. Computational Fluid Dynamics analysis of wind turbine blade at various angles of attack and different Reynolds number. Procedia Eng, 127: 1363-1369.

- REN21-Renewable Energy Policy Network for the 21st Century. 2018. Renewables 2018 Global Status Report. Paris, France.
- Sagol E, Reggio M, Ilinca A. 2013. Issues concerning roughness on wind turbine blades. *Renewable Sustain Energy Rev*, 23: 514-525.
- Salem H, Diab A, Ghoneim Z. 2013. CFD simulation and analysis of performance degradation of wind turbine blades in dusty environments. In *2013 International Conference on Renewable Energy Research and Applications*; 20-23 October 2013, Madrid, Spain.
- Sayed MA, Kandil HA, Morgan ESI. 2012. Computational fluid dynamics study of wind turbine blade profiles at low Reynolds numbers for various angles of attack. In *AIP Conference Proceedings*, 1440: 467-479.
- Timmer WA, Rooij RPJOM. 2003. Summary of the Delft University wind turbine dedicated airfoils. In *41st Aerospace Sciences Meeting and Exhibit*; 6-9 January 2003, Reno, Nevada, USA.
- Villalpando F, Reggio M, Ilinca A. 2012. Numerical study of flow around iced wind turbine airfoil. *EACFM*, 6(1): 39-45.
- Vendan SP, AravindLovelin S, Manibharathi M, Rajkumar C. 2010. Analysis of a wind turbine blade profile for tapping wind power at the regions of low wind speed. *IJME*, 2: 1-10.
- Yilmaz I, Cam O, Tastan, M, Karci, A. 2016. Experimental investigation of aerodynamic performance of different wind turbine airfoils. *J Polytech*, 19(4): 577-584.
- Wilcox DC. 2006. *Turbulence Modeling for CFD*. 3rd ed. California, USA: DCW Industries.